

Controlled pairing symmetries in a Fermi-Hubbard ladder with band flattening

João P. Mendonça,^{1,2,*} S. Biswas,³ M. Dziurawiec,⁴ U. Bhattacharya,⁵ K. Jachymski,² M. Aidelsburger,^{6,7,8} M. Lewenstein,⁹ M. M. Maśka,⁴ and T. Grass^{3,10,†}

¹*Centre for Quantum Optical Technologies, Centre of New Technologies, University of Warsaw, Banacha 2c, 02-097 Warsaw, Poland*

²*Faculty of Physics, University of Warsaw, Pasteura 5, 02-093 Warsaw, Poland*

³*DIPC - Donostia International Physics Center, Paseo Manuel de Lardizábal 4, 20018 San Sebastián, Spain*

⁴*Institute of Theoretical Physics, Wrocław University of Science and Technology, 50-370 Wrocław, Poland*

⁵*Institute for Theoretical Physics, ETH Zürich, Zürich 8093, Switzerland*

⁶*Max-Planck-Institut für Quantenoptik, 85748 Garching, Germany*

⁷*Munich Center for Quantum Science and Technology (MCQST), 80799 München, Germany*

⁸*Fakultät für Physik, Ludwig-Maximilians-Universität, 80799 München, Germany*

⁹*ICFO-Institut de Ciències Fotoniques, The Barcelona Institute of Science and Technology, 08860 Castelldefels (Barcelona), Spain*

¹⁰*IKERBASQUE, Basque Foundation for Science, Plaza Euskadi 5, 48009 Bilbao, Spain*

(Dated: December 25, 2025)

Band flattening has been identified as key ingredient to correlation phenomena in Moiré materials and beyond. Here, we examine strongly repulsive fermions on a ladder – a minimal platform for unconventional d -wave pairing – and show that flattening of the lower band through an additional diagonal hopping term produces non-Fermi liquid behavior, evidenced by the violation of Luttinger’s theorem, as well as axial d -wave pairing correlations. Alternatively, plaquette ring exchange can also generate pairing, albeit with a distinct diagonal d -wave pairing symmetry. Hence, our finding showcases a competition of different unconventional pairing channels, and demonstrates via a simple model how band geometry can induce fermionic pairing. This offers broadly relevant insights for correlated flat-band systems, ranging from ultracold atoms to strongly interacting electrons in solids.

Introduction. Since the discovery of twisted bilayer graphene at the magic angle [1], flat energy bands have become a central paradigm in the search for strongly correlated phases, both in electronic systems [2–6] and in synthetic quantum matter [7–10]; see Ref. 11 for a review. While twisting offers a powerful route to band flattening, geometric control in single-layer systems provides an alternative and conceptually simpler mechanism. Prominent examples include the Lieb and Kagome lattices, where flat bands arise naturally and have stimulated extensive studies of flat-band Bose–Einstein condensation [12–14]. From a theoretical standpoint, one of the simplest settings with tunable bandwidth is a two-leg ladder in square geometry augmented by a diagonal next-nearest-neighbor hopping t_d , cf. Fig. 1(a). The resulting band structure consists of two bands with bandwidths $2|t_h \pm t_d|$, where t_h denotes hopping along the legs. By tuning t_d , one band can be continuously flattened and even rendered exactly dispersionless, as shown in Figs. 1(b)–(d). This construction offers a minimal and highly controllable route to flat-band physics. Crucially, the two-leg ladder is also the minimal geometry that extends one-dimensional systems into a second dimension, thereby permitting spatially nontrivial pairing correlations. In particular, it naturally supports d -wave symmetry. Jiang *et al.* [15] demonstrated that robust d -wave correlations can be stabilized in this geometry by introducing a ring-exchange interaction K , which coherently transfers an electronic singlet between the two diagonals of a plaquette. Related bosonic studies revealed analogo-

gous d -wave correlations and identified the ladder as a promising route toward Bose-metal behavior [16–19], an elusive non-condensed phase with a recently proposed realization in trapped-ion platforms [20]. In the fermionic case—where the state may be viewed as a product of a bosonic d -wave phase of chargons and a Slater determinant of spinons [15]—the emergence of d -wave pairing is accompanied by a fundamental reconstruction of the electronic structure. Most notably, Luttinger’s theorem is violated [21], signaling the breakdown of the conventional Fermi sea and the onset of a non-Fermi-liquid (NFL) phase. However, access to this regime requires a ring-exchange strength comparable to the bare hopping, posing a practical limitation. This observation motivates the central idea of this work: combining ring-exchange interactions with band flattening to amplify correlation effects.

In this Letter, we develop this idea by studying a Fermi–Hubbard ladder with diagonal hopping t_d and ring-exchange interactions K . For $0 > t_d > -0.5t_h$, the width of the lower band is reduced while a finite band gap is preserved, see Fig. 1(c). Focusing on this regime, we show that diagonal hopping provides a natural and experimentally relevant knob to enhance pairing tendencies and stabilize non-Fermi-liquid (NFL) behavior at significantly reduced interaction strengths. Moreover, we find that the NFL regime splits into two distinct phases, most clearly distinguished by their d -wave pairing symmetries. While ring-exchange interactions favor diagonal d_{xy} -wave pairing, diagonal hopping promotes axial $d_{x^2-y^2}$ -wave

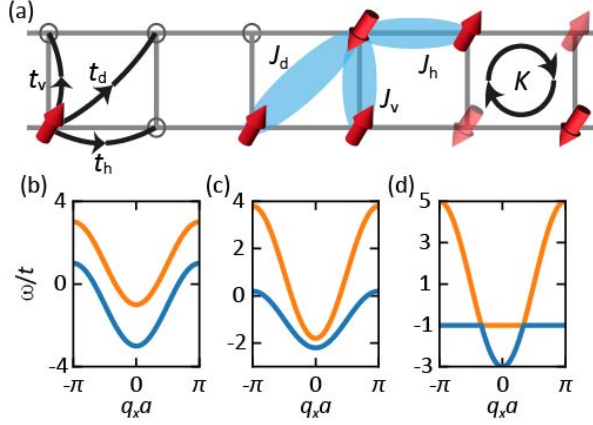


FIG. 1. (a) Schematic representation of the extended t - J - K model [cf. Eq. (1)]. Electrons are allowed to hop between all neighboring sites, including horizontal, vertical, and diagonals. The exchange interaction is tied to the hoppings via $J = 4t^2/U$. The ring-exchange interaction acting on a single plaquette is shown. (b-d): Single-particle bands for (b) $t_d = 0$, (c) $t_d = -0.4$, and (d) $t_d = -1$ (in units of $t = t_h = t_v$).

correlations. Our results thus reveal a direct competition between interaction-driven and geometry-induced pairing mechanisms and establish, within a minimal model, how band flattening via diagonal hopping enhances fermionic pairing in ladder systems. These findings are directly relevant for experiments with ultracold atoms [22], quantum dot arrays [23], and quasi-one-dimensional, multi-orbital strongly correlated materials [24, 25]. We further note that artificial gauge fields have achieved complex or negative tunneling amplitudes in optical lattice experiments, including systems with synthetic ladder geometry [26–33]. More broadly, our work provides a transparent example of how band flattening can qualitatively reshape correlated many-body phases, even in simple lattice geometries.

Model. Following earlier work on NFL d -wave phase [15], we assume a strongly repulsive Fermi-Hubbard system that is faithfully described by the t - J model, disregarding states with doubly occupied sites, thereby limiting the interactions to a second-order exchange process $J_{ij} = 4t_{ij}^2/U$, where i, j are site indices, and the interaction is strong, $U \gg t$. As indicated in Fig. 1(a), we assume non-zero hopping terms (t_h , t_v , t_d) as well as non-zero exchange terms (J_h , J_v , J_d) for nearest neighbors along the leg and rung, as well as next-nearest neighbors along the diagonals of each plaquette. Throughout this paper, we set $U = 2$ and $t_h = t_v = t = 1$, while t_d is kept tunable. While we focus on the two-leg ladder structure, the model has also received attention in the 2D context [34, 35], where pairing tendencies can condense into true long-range superconducting order. In addition to hopping and exchange

terms, we also include a tunable ring exchange term K . The total t - J - K Hamiltonian reads:

$$H = - \sum_{\langle i,j \rangle, \sigma} t_{ij} (\hat{c}_{i\sigma}^\dagger \hat{c}_{j\sigma} + \text{H.c.}) + \sum_{\langle i,j \rangle} J_{ij} \hat{S}_i \cdot \hat{S}_j + 2K \sum_{\square} (\hat{\Delta}_{13}^\dagger \hat{\Delta}_{24} + \text{H.c.}), \quad (1)$$

where $\hat{\Delta}_{ij}^\dagger = (\hat{c}_{i\uparrow}^\dagger \hat{c}_{j\downarrow}^\dagger - \hat{c}_{i\downarrow}^\dagger \hat{c}_{j\uparrow}^\dagger)/\sqrt{2}$. The spin operators are defined as $\hat{S}_i = \frac{1}{2} \sum_{\sigma, \sigma'} \hat{c}_{i\sigma}^\dagger \sigma_{\sigma\sigma'} \hat{c}_{i\sigma'}$. The sums are carried out over nearest-neighbor sites $\langle i, j \rangle$, and along elementary plaquettes \square . For simplicity, and as done in earlier work [15], we have neglected the $-J\hat{n}_i\hat{n}_j/4$ term of the standard t - J model.

Non-Fermi liquid phases. Using DMRG calculations [36], we first analyze the momentum distribution $\langle n_{\uparrow}(\mathbf{q}) \rangle = \langle \hat{c}_{\mathbf{q},\uparrow}^\dagger \hat{c}_{\mathbf{q},\uparrow} \rangle$. In a Fermi liquid (FL), the momentum distribution obeys the Luttinger liquid (LL) theorem and exhibits a singular surface associated with the Fermi sea, with a non-analyticity at the Fermi wavevector $k_F = \pi\rho$. The particle density is $\rho = N_e/N$, where $N_e = N_\uparrow + N_\downarrow$ and $N = 2L_x$. Throughout this work, we fix $\rho = 1/3$. The FL momentum distribution is shown in Fig. 2(a) for $t_d = -0.1$ and $K = 0.5$, where only modes with $q_y = 0$ and $|q_x| \lesssim k_F$ are occupied. Increasing K drives a sharp qualitative change in $\langle n_{\uparrow}(\mathbf{q}) \rangle$ as the system enters a NFL regime. As illustrated in Fig. 2(b) for $t_d = -0.1$ and $K = 1.4$, the momentum distribution no longer displays a well-defined Fermi surface, signaling a strong breakdown of the LL theorem. The nature of the FL-NFL transition is made explicit by the derivative $|\partial_{q_x} \langle n_{\uparrow}(\mathbf{q}) \rangle|$, shown in Fig. 2(c) as a function of K . In the FL phase, the dominant peaks are pinned to $|q_x| = k_F$. By contrast, in the d_{xy} -NFL regime these peaks shift abruptly to incommensurate momenta, providing a clear and unambiguous signature of a strong violation of the LL theorem. At stronger diagonal hopping, $t_d = -0.3$, the violation of the LL theorem takes a qualitatively different form. As shown in Fig. 2(f), deviations from FL behavior emerge already for $K \gtrsim 0.5$, but now through a continuous evolution of the peak positions rather than an abrupt jump. The corresponding momentum distribution at intermediate coupling, Fig. 2(d) for $K = 0.65$, exhibits a weak population of the $q_y = \pi$ sector, $0 < \langle n_{\uparrow}(q_x, \pi) \rangle < 1$ at small q_x , together with a reduced $q_y = 0$ plateau terminating at $q_x < k_F$. This smooth redistribution of spectral weight indicates a weak violation of the LL theorem. Upon further increasing K , the system crosses over into a regime with pronounced NFL character. As shown in Fig. 2(e) for $K = 1.2$, the momentum distribution departs strongly from FL behavior and closely resembles the strongly violating d_{xy} -NFL phase of Fig. 2(b). In summary, the momentum distribution reveals two distinct mechanisms by which the LL theorem is violated: a *weak* violation characterized by a continuous deformation of the Fermi surface and a grad-

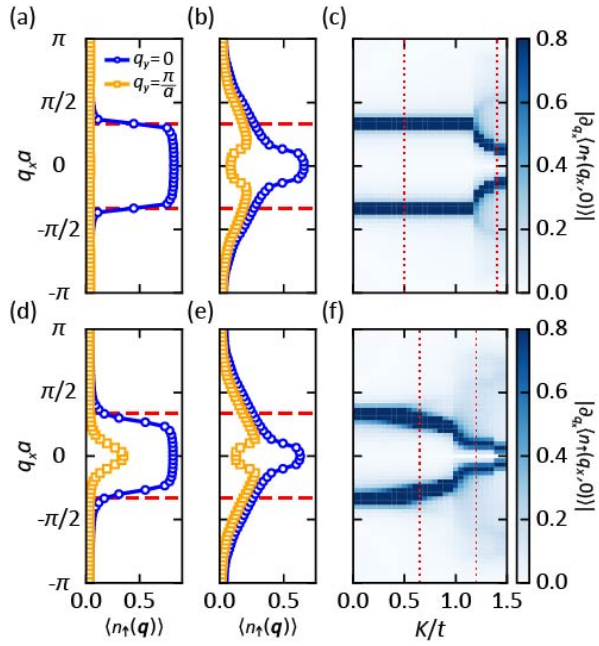


FIG. 2. (a,b,d,e) Momentum distribution $\langle \hat{n}_\uparrow(\mathbf{q}) \rangle$ for $L_x = 30$, and fixed (a-c) $t_d = -0.1$ and (d-f) $t_d = -0.3$. (a) Shows FL behavior at $K = 0.5$, whereas panel (b) NFL behavior at $K = 1.4$. Both (d) at $K = 0.65$ and (e) at $K = 1.2$ showcase distinct NFL behavior. In panels (c,f) the absolute value of the derivative $\partial \langle \hat{n}_\uparrow(q_x, 0) \rangle / \partial q_x$ is plotted as a function of q_x and K for $q_y = 0$. Dotted lines in (c,f) mark the K values which are shown in panels (a,b,d,e). The Fermi wave vector k_F is represented by horizontal red dashed lines.

ual redistribution of spectral weight, and a *strong* violation marked by abrupt shifts of the singular momenta and the disappearance of a well-defined Fermi surface. These two regimes correspond, respectively, to $d_{x^2-y^2}$ - and d_{xy} -wave NFL phases, as we will show below by analyzing their pairing symmetries.

Transitions between different phases can also be identified using dynamical properties, providing us with not only additional characteristics of the NFL nature of these phases, but also data that are particularly important in light of recent advances in experimental methods such as INS, RIXS and ARPES [37, 38]. These methods allow for the measurement of the response of quantum many-body systems at specific energies and momenta, and specifically of the spectral function (cf. [39]), analyzed in Fig. 3. Panels (a) and (b) show two examples of the spectral function in two distinct NFL regimes. Importantly, both regimes are characterized by a gap δ that opens at momentum $k_L < k_F$, approximately coinciding with the peak of the derivative $|\partial_{q_x} \langle n_\uparrow(q_x, 0) \rangle|$ analyzed in Fig. 2(c,f). The gap δ and the momentum k_L as a function of K are shown in Fig. 3 (c) and (d) for moderate diagonal hopping $t_d = -0.25$. We notice that the opening of a gap coincides with the onset of LL theorem violation, marked by the dotted horizontal lines. This

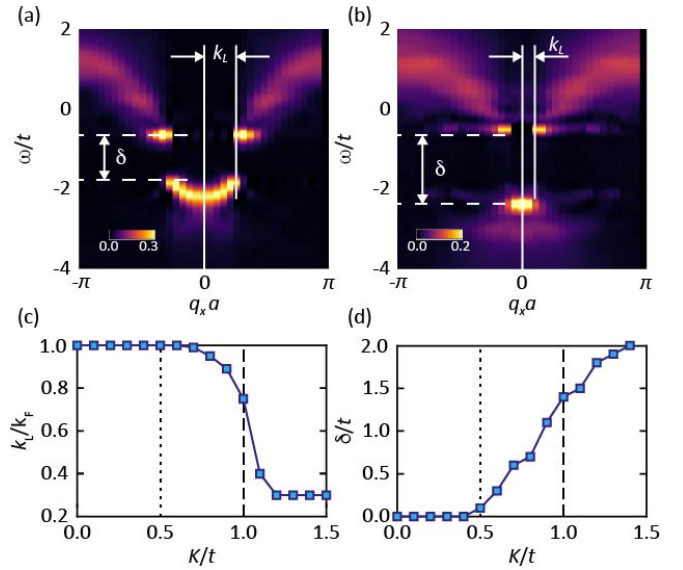


FIG. 3. Spectral function analysis for $t_d = -0.25$, $q_y = 0$, and $L_x = 36$. Two representative values are shown in (a) $K = 0.8$ and (b) $K = 1.2$. (c) Gap δ and (d) corresponding momentum k_L , schematically shown in the (a)-(b), as a function of K . Vertical lines correspond to FL-NFL transition points.

behavior corresponds to the transition from the FL to NFL. We further notice a sharp drop in k_L at $K \approx 1$, marked by the vertical dashed line. This drop separates the $d_{x^2-y^2}$ -wave NFL regime, in which the LL theorem is weakly violated, from the d_{xy} -wave NFL regime, characterized by strong NFL behavior. These differences are qualitatively observed in panels (a) and (b) of Fig. 3: While in Fig. 3(a) we observe a gapped phase with well-defined dispersion, corresponding to the (weak) $d_{x^2-y^2}$ -wave NFL phase, Fig. 3(b) shows a more complex structure, characteristic for the (strong) d_{xy} -wave NFL phase.

Pairing correlations. With the complementary observables introduced so far, we have differentiated between three phases: FL, weak NFL, and strong NFL. As we show in the following, the distinction between these phases, and in particular between the different NFL regions, becomes clearest if we consider pairing correlations. In the absence of the band flattening term, the NFL phase has been identified as d -wave because of the d -wave symmetry exhibited by its Cooper-pair correlations [15]. As we show below, different pairing channels become relevant in the model with diagonal hopping. To identify the type of pairing, we analyze the singlet-pairing density matrix. In general, this quantity reads

$$\rho_S(\mathbf{r}_i, \mathbf{r}_j | \mathbf{r}_k, \mathbf{r}_l) = \langle \hat{\Delta}_{ij}^\dagger \hat{\Delta}_{kl} \rangle. \quad (2)$$

To exclude local contributions from density and spin correlations, we set the density matrix $\rho_S(\mathbf{r}_i | \mathbf{r}_j)$ to zero whenever there is overlap of Cooper pairs that share a site [40]. Therefore, ρ_S is no longer positive definite, so some of its eigenvalues may be negative. For the d -wave

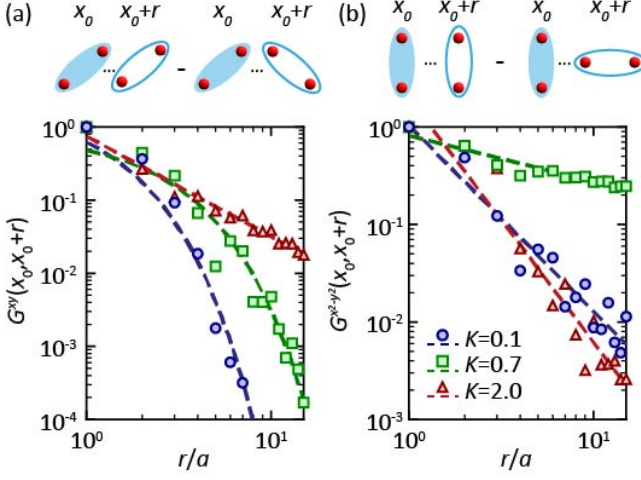


FIG. 4. Pair correlations for the two d -wave channels for $t_d = -0.25$, $L_x = 30$, and three distinct values of K , representative of the three phases. (a) Diagonal (alias d_{xy}) and (b) axial (alias $d_{x^2-y^2}$) d -wave pair correlations, as schematically illustrated in the top panels. Dashed curves represent the best numerical fit between power-law and exponential. Correlations are renormalized to the first point to better illustrate the decay laws.

pairing, two channels are taken into account in our geometry:

$$G_{ij}^{xy} = \rho_S(\mathbf{r}_i, \mathbf{r}_i + \hat{\mathbf{x}} + \hat{\mathbf{y}} | \mathbf{r}_j, \mathbf{r}_j + \hat{\mathbf{x}} + \hat{\mathbf{y}}) - \rho_S(\mathbf{r}_i, \mathbf{r}_i + \hat{\mathbf{x}} + \hat{\mathbf{y}} | \mathbf{r}_j + \hat{\mathbf{y}}, \mathbf{r}_j + \hat{\mathbf{x}}), \quad (3a)$$

$$G_{ij}^{x^2-y^2} = \rho_S(\mathbf{r}_i, \mathbf{r}_i + \hat{\mathbf{y}} | \mathbf{r}_j, \mathbf{r}_j + \hat{\mathbf{y}}) - \rho_S(\mathbf{r}_i, \mathbf{r}_i + \hat{\mathbf{y}} | \mathbf{r}_j, \mathbf{r}_j + \hat{\mathbf{x}}), \quad (3b)$$

with the first representing *diagonal* d -wave (xy) pairs while the second depicts *axial* d -wave (x^2-y^2) pairs. We show a visual representation in Fig. 4 and plot the correlations as a function of distance $r = |\mathbf{r}_i - \mathbf{r}_j|$ within the bulk. In this figure, $t_d = -0.25$ is fixed, and we choose three values of K as representatives of the three regimes identified earlier (Fermi-liquid and two NFL phases), allowing a direct visual comparison between the character of pair correlations across phases. Fig. 4(a) shows the diagonal d_{xy} -wave correlations, which change qualitatively from an exponential decay at small and moderate K to a clear algebraic tail at strong ring exchange interaction, signaling the emergence of quasi-long-range order in the strong-NFL region. In contrast, Fig. 4(b) displays the axial $d_{x^2-y^2}$ channel, where the correlations show a slow, almost flat, decay with distance r for moderate K , while a faster than polynomial decay is observed in both the FL and strong-NFL regimes. The dashed lines represent the best numerical fits distinguishing the exponential and power-law decay laws. Although blurred by finite-size effects, a clear distinction is observed between short- and long-range correlations.

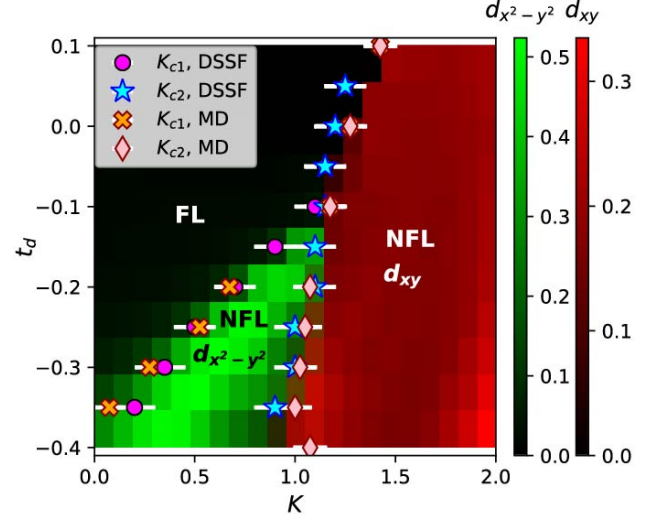


FIG. 5. Finite-size phase diagram depicting the three main phases observed: a Fermi-liquid phase (FL) and two non-Fermi-liquid (NFL) phases with distinct d -wave pairing symmetries. The color background shows the eigenvalue gap in the dominant pairing channel, i.e. $d_{x^2-y^2}$ (green) or d_{xy} (red). As indicated by the symbols, the phase boundaries can also be obtained from inspection of the momentum distribution (MD) and the dynamical spin structure factor (DSSF), where critical values K_{c1} and K_{c2} mark the transitions between the different phases. The grid of K values in the calculation yields horizontal error bars.

A clear theoretical signature of fragmented Cooper-pair condensation is provided by the generalized Penrose–Onsager criterion [41, 42]. The emergence of Cooper-pair condensation in a given pairing channel is signaled by a dominant eigenvalue ε_n of the corresponding pairing density matrix, $\rho_S(\mathbf{r}_i | \mathbf{r}_j) = \sum_n \varepsilon_n \chi_n^*(\mathbf{r}_i) \chi_n(\mathbf{r}_j)$, which directly encodes the behavior of G_{ij}^{ξ} . The eigenvalue gap $\varepsilon_0 - \varepsilon_1$ therefore serves as a sensitive diagnostic for identifying pairing symmetry, as illustrated in Fig. 5. We find that these gaps remain robust upon increasing system size (see Supplemental Material [39]), where we also present the full eigenvalue spectra across the different phases.

Implementation. In physical systems, ring-exchange interactions can arise from nonlocal interaction potentials. In neutral-atom quantum simulation experiments, such processes typically emerge only at higher order, as demonstrated, for example, in Ref. [43]. Identifying schemes that enhance the energy scale of ring-exchange interactions has long been a central challenge in quantum simulation, particularly in the context of lattice gauge theories [44]. In contrast, sizeable negative diagonal hopping amplitudes appear to be directly accessible with state-of-the-art Floquet engineering techniques or by exploiting synthetic dimensions (cf. Refs. 45–48). In particular, diagonal tunneling couplings with tunable complex amplitudes have been demonstrated in simulations

of Creutz ladders [31] and in Raman-coupled lattices [30]. We note, however, that engineering the required interaction terms is more challenging in approaches based on synthetic dimensions. A well-known limitation of Floquet systems is heating, especially in the presence of interactions, which has so far constrained progress toward realizing strongly correlated topological phases of matter. Recent experiments, however, have reported the realization of large Floquet many-body systems of strongly interacting bosonic atoms subject to artificial gauge fields at temperatures on the order of the tunneling energy [33], underscoring the experimental feasibility of our proposed scheme. To assess on the thermal stability of the $d_{x^2-y^2}$ pairing phase at these temperatures, we calculated the pairing gap, see SM [39], and show that a gap larger than $0.5t$ can be achieved. Importantly, one of these ingredients – either diagonal hopping or ring exchange – is sufficient to drive a transition from a FL into a NFL d -wave pairing phase, hence our manuscript outlines two different avenues to achieve the outstanding goal of realizing and controlling pairing physics in Fermi-Hubbard systems and directly connects to recent experimental efforts in engineering low-entropy phases in the Fermi-Hubbard model with next-nearest-neighbor tunneling [49].

Summary. We find that ring-exchange interactions combined with negative diagonal hopping in a strongly repulsive Fermi-Hubbard ladder stabilize distinct non-Fermi-liquid phases, characterized by the breakdown of Luttinger liquid theory, quasi-long-range d -wave-like correlations, and fragmented Cooper-pair condensation. Our minimal model elucidates how band flattening generates competition among pairing symmetries. Identifying diagonal tunneling as an efficient route to stabilize d -wave pairing, our results open new perspectives for engineered synthetic matter systems.

Acknowledgments. We thank Ravindra Chhajlany and Tymoteusz Salamon for the fruitful discussions in the early stages of the project. J.P.M. and K.J. were supported by the Polish National Agency for Academic Exchange (NAWA) via the Polish Returns 2019 program and gratefully acknowledge Polish high-performance computing infrastructure PLGrid (HPC Center: ACK Cyfronet AGH) for providing computer facilities and support within computational grant no. PLG/2024/017478. Part of the numerical calculations have also been carried out using the resources provided by the Wrocław Centre for Networking and Supercomputing. The "Quantum Optical Technologies" (FENG.02.01-IP.05-0017/23) project is carried out within the Measure 2.1 International Research Agendas programme of the Foundation for Polish Science, co-financed by the European Union under the European Funds for Smart Economy 2021-2027 (FENG). M.M.M. acknowledges support from the National Science Centre (Poland) under Grant No. 2024/53/B/ST3/02756. M.D. acknowledges support from the National Science Centre (Poland) under Grant

No. 2022/04/Y/ST3/00061. M.A. acknowledges support from the Deutsche Forschungsgemeinschaft (DFG, German Research Foundation) under Germany's Excellence Strategy – EXC-2111 – 390814868 and the Horizon Europe programme HORIZON-CL4-2022-QUANTUM-02-SGA via the project 101113690 (PASQuanS2.1). T.G. acknowledges funding by the Department of Education of the Basque Government through the IKUR Strategy, through BasQ (project EMISGALA), and through PIBA.2023.1.0021 (TENINT), and by the Agencia Estatal de Investigación (AEI) through Proyectos de Generación de Conocimiento PID2022-142308NA-I00 (EXQUSMI). This work has been produced with the support of a 2023 Leonardo Grant for Researchers in Physics, BBVA Foundation. The BBVA Foundation is not responsible for the opinions, comments, and contents included in the project and/or the results derived therefrom, which are the total and absolute responsibility of the authors.

* jpedromend@gmail.com

† tobias.grass@dipc.org

- [1] Y. Cao, V. Fatemi, A. Demir, S. Fang, S. L. Tomarken, J. Y. Luo, J. D. Sanchez-Yamagishi, K. Watanabe, T. Taniguchi, E. Kaxiras, R. C. Ashoori, and P. Jarillo-Herrero, Correlated insulator behaviour at half-filling in magic-angle graphene superlattices, *Nature* **556**, 80 (2018).
- [2] L. Wang, E.-M. Shih, A. Ghiotto, L. Xian, D. A. Rhodes, C. Tan, M. Claassen, D. M. Kennes, Y. Bai, B. Kim, K. Watanabe, T. Taniguchi, X. Zhu, J. Hone, A. Rubio, A. N. Pasupathy, and C. R. Dean, Correlated electronic phases in twisted bilayer transition metal dichalcogenides, *Nature Materials* **19**, 861 (2020).
- [3] Z. Zhang, Y. Wang, K. Watanabe, T. Taniguchi, K. Ueno, E. Tutuc, and B. J. LeRoy, Flat bands in twisted bilayer transition metal dichalcogenides, *Nature Physics* **16**, 1093 (2020).
- [4] A. Uri, S. C. de la Barrera, M. T. Randeria, D. Rodan-Legrain, T. Devakul, P. J. D. Crowley, N. Paul, K. Watanabe, T. Taniguchi, R. Lifshitz, L. Fu, R. C. Ashoori, and P. Jarillo-Herrero, Superconductivity and strong interactions in a tunable moiré quasicrystal, *Nature* **620**, 762 (2023).
- [5] Y. Li, F. Zhang, V.-A. Ha, Y.-C. Lin, C. Dong, Q. Gao, Z. Liu, X. Liu, S. H. Ryu, H. Kim, C. Jozwiak, A. Bostwick, K. Watanabe, T. Taniguchi, B. Kousa, X. Li, E. Rotenberg, E. Khalaf, J. A. Robinson, F. Giustino, and C.-K. Shih, Tuning commensurability in twisted van der Waals bilayers, *Nature* **625**, 494 (2024).
- [6] C.-Y. Hao, Z. Zhan, P. A. Pantaleón, J.-Q. He, Y.-X. Zhao, K. Watanabe, T. Taniguchi, F. Guinea, and L. He, Robust flat bands in twisted trilayer graphene moiré quasicrystals, *Nat. Commun.* **15**, 8437 (2024).
- [7] A. González-Tudela and J. I. Cirac, Cold atoms in twisted-bilayer optical potentials, *Phys. Rev. A* **100**, 053604 (2019).
- [8] T. Salamon, A. Celi, R. W. Chhajlany, I. Frérot, M. Lewenstein, L. Tarruell, and D. Rakshit, Simulating

twistrionics without a twist, *Phys. Rev. Lett.* **125**, 030504 (2020).

[9] T. Salamon, B. Irsigler, D. Rakshit, M. Lewenstein, T. Grass, and R. Chhajlany, Flat-band-induced superconductivity in synthetic bilayer optical lattices, *Phys. Rev. B* **106**, 174503 (2022).

[10] Z. Meng, L. Wang, W. Han, F. Liu, K. Wen, C. Gao, P. Wang, C. Chin, and J. Zhang, Atomic bose-einstein condensate in twisted-bilayer optical lattices, *Nature* **615**, 231 (2023).

[11] P. Törmä, S. Peotta, and B. A. Bernevig, Superconductivity, superfluidity and quantum geometry in twisted multilayer systems, *Nature Reviews Physics* **4**, 528 (2022).

[12] Y.-Z. You, Z. Chen, X.-Q. Sun, and H. Zhai, Superfluidity of bosons in kagome lattices with frustration, *Phys. Rev. Lett.* **109**, 265302 (2012).

[13] A. Julku, G. M. Bruun, and P. Törmä, Quantum geometry and flat band bose-einstein condensation, *Phys. Rev. Lett.* **127**, 170404 (2021).

[14] Z. Jalali-mola, T. Grass, V. Kasper, M. Lewenstein, and U. Bhattacharya, Topological bogoliubov quasiparticles from bose-einstein condensate in a flat band system, *Phys. Rev. Lett.* **131**, 226601 (2023).

[15] H.-C. Jiang, M. S. Block, R. V. Mishmash, J. R. Garrison, D. Sheng, O. I. Motrunich, and M. P. Fisher, Non-fermi-liquid d -wave metal phase of strongly interacting electrons, *Nature* **493**, 39 (2013).

[16] O. I. Motrunich and M. P. A. Fisher, d -wave correlated critical bose liquids in two dimensions, *Phys. Rev. B* **75**, 235116 (2007).

[17] D. N. Sheng, O. I. Motrunich, S. Trebst, E. Gull, and M. P. A. Fisher, Strong-coupling phases of frustrated bosons on a two-leg ladder with ring exchange, *Phys. Rev. B* **78**, 054520 (2008).

[18] R. V. Mishmash, M. S. Block, R. K. Kaul, D. N. Sheng, O. I. Motrunich, and M. P. A. Fisher, Bose metals and insulators on multileg ladders with ring exchange, *Phys. Rev. B* **84**, 245127 (2011).

[19] S. Biswas, E. Rico, and T. Grass, Frustrated bose ladder with extended range density-density interaction, *Phys. Rev. B* **112**, 115122 (2025).

[20] S. Biswas, E. Rico, and T. Grass, Ring-exchange physics in a chain of three-level ions, *Quantum* **9**, 1683 (2025).

[21] J. M. Luttinger, Fermi surface and some simple equilibrium properties of a system of interacting fermions, *Phys. Rev.* **119**, 1153 (1960).

[22] S. Hirthe, T. Chalopin, D. Bourgund, P. Bojović, A. Bohrdt, E. Demler, F. Grusdt, I. Bloch, and T. A. Hilker, Magnetically mediated hole pairing in fermionic ladders of ultracold atoms, *Nature* **613**, 463 (2023).

[23] T.-K. Hsiao, P. Cova Fariña, S. D. Oosterhout, D. Jirovec, X. Zhang, C. J. van Diepen, W. I. L. Lawrie, C.-A. Wang, A. Sammak, G. Scappucci, M. Veldhorst, E. Demler, and L. M. K. Vandersypen, Exciton transport in a germanium quantum dot ladder, *Phys. Rev. X* **14**, 011048 (2024).

[24] J. Herbrych, N. Kaushal, A. Nocera, G. Alvarez, A. Moreo, and E. Dagotto, Spin dynamics of the block orbital-selective mott phase, *Nature Communications* **9**, 3736 (2018).

[25] J. Herbrych, J. Heverhagen, N. D. Patel, G. Alvarez, M. Daghofer, A. Moreo, and E. Dagotto, Novel magnetic block states in low-dimensional iron-based superconductors, *Phys. Rev. Lett.* **123**, 027203 (2019).

[26] M. Atala, M. Aidelsburger, M. Lohse, J. T. Barreiro, B. Paredes, and I. Bloch, Observation of chiral currents with ultracold atoms in bosonic ladders, *Nature Physics* **10**, 588 (2014).

[27] B. K. Stuhl, H.-I. Lu, L. M. Aycock, D. Genkina, and I. B. Spielman, Visualizing edge states with an atomic bose gas in the quantum hall regime, *Science* **349**, 1514 (2015), <https://www.science.org/doi/pdf/10.1126/science.aaa8515>.

[28] M. Mancini, G. Pagano, G. Cappellini, L. Livi, M. Rider, J. Catani, C. Sias, P. Zoller, M. Inguscio, M. Dalmonte, and L. Fallani, Observation of chiral edge states with neutral fermions in synthetic hall ribbons, *Science* **349**, 1510 (2015), <https://www.science.org/doi/pdf/10.1126/science.aaa8736>.

[29] M. E. Tai, A. Lukin, M. Rispoli, R. Schittko, T. Menke, D. Borgnia, P. M. Preiss, F. Grusdt, A. M. Kaufman, and M. Greiner, Microscopy of the interacting harper-hofstadter model in the two-body limit, *Nature* **546**, 519 (2017).

[30] B. Song, L. Zhang, C. He, T. F. J. Poon, E. Hajiyev, S. Zhang, X.-J. Liu, and G.-B. Jo, Observation of symmetry-protected topological band with ultracold fermions, *Science Advances* **4**, eaao4748 (2018).

[31] J. H. Kang, J. H. Han, and Y. Shin, Creutz ladder in a resonantly shaken 1D optical lattice, *New Journal of Physics* **22**, 013023 (2020).

[32] T.-W. Zhou, G. Cappellini, D. Tusi, L. Franchi, J. Parravicini, C. Repellin, S. Greschner, M. Inguscio, T. Giamarchi, M. Filippone, J. Catani, and L. Fallani, Observation of universal hall response in strongly interacting fermions, *Science* **381**, 427 (2023), <https://www.science.org/doi/pdf/10.1126/science.add1969>.

[33] A. Impertro, S. Huh, S. Karch, J. F. Wienand, I. Bloch, and M. Aidelsburger, Strongly interacting meissner phases in large bosonic flux ladders, *Nature Physics* **21**, 895 (2025).

[34] S. Gong, W. Zhu, and D. N. Sheng, Robust d -wave superconductivity in the square-lattice $t-j$ model, *Phys. Rev. Lett.* **127**, 097003 (2021).

[35] S. Jiang, D. J. Scalapino, and S. R. White, Ground-state phase diagram of the $t-t'-j$ model, *Proceedings of the National Academy of Sciences* **118**, e2109978118 (2021).

[36] The numerical simulations in this work were performed using the ITensors library in Julia [50, 51]. The energy convergence tolerance was set to 10^{-10} , and results were recorded only after reaching this precision. The truncation error was controlled by a cutoff of 10^{-10} , yielding a maximum truncation error of approximately 10^{-10} in the final DMRG sweeps.

[37] J. A. Sobota, Y. He, and Z.-X. Shen, Angle-resolved photoemission studies of quantum materials, *Rev. Mod. Phys.* **93**, 025006 (2021).

[38] M. Mitrano, S. Johnston, Y.-J. Kim, and M. P. M. Dean, Exploring quantum materials with resonant inelastic x-ray scattering, *Phys. Rev. X* **14**, 040501 (2024).

[39] See the Supplemental Material (SM), including references [52, 53], for additional information related to dynamical properties (spectral function, dynamical spin structure factor), to the generalized Penrose-Onsager criterion, obtained from the eigenvalue spectrum of the non-local d -wave density matrices, and on the finite-size scaling of the eigenvalue gaps.

[40] A. Wietek, Fragmented cooper pair condensation in striped superconductors, *Phys. Rev. Lett.* **129**, 177001 (2022).

[41] O. Penrose and L. Onsager, Bose-einstein condensation and liquid helium, *Phys. Rev.* **104**, 576 (1956).

[42] A. Leggett, *Quantum Liquids: Bose Condensation and Cooper Pairing in Condensed-matter Systems*, Oxford Graduate Texts (OUP Oxford, 2006).

[43] H.-N. Dai, B. Yang, A. Reingruber, H. Sun, X.-F. Xu, Y.-A. Chen, Z.-S. Yuan, and J.-W. Pan, Four-body ring-exchange interactions and anyonic statistics within a minimal toric-code Hamiltonian, *Nature Physics* **13**, 1195 (2017).

[44] J. Feldmeier, N. Maskara, N. U. Köylüoğlu, and M. D. Lukin, Quantum simulation of dynamical gauge theories in periodically driven Rydberg atom arrays, arXiv:2408.02733 10.48550/arXiv.2408.02733 (2024), arXiv:2408.02733.

[45] N. Goldman and J. Dalibard, Periodically driven quantum systems: Effective hamiltonians and engineered gauge fields, *Phys. Rev. X* **4**, 031027 (2014).

[46] A. Celi, P. Massignan, J. Ruseckas, N. Goldman, I. B. Spielman, G. Juzeliūnas, and M. Lewenstein, Synthetic Gauge Fields in Synthetic Dimensions, *Phys. Rev. Lett.* **112**, 043001 (2014).

[47] T. Graß, C. Muschik, A. Celi, R. W. Chhajlany, and M. Lewenstein, Synthetic magnetic fluxes and topological order in one-dimensional spin systems, *Phys. Rev. A* **91**, 063612 (2015).

[48] A. Eckardt, Colloquium: Atomic quantum gases in periodically driven optical lattices, *Rev. Mod. Phys.* **89**, 011004 (2017).

[49] M. Xu, L. H. Kendrick, A. Kale, Y. Gang, C. Feng, S. Zhang, A. W. Young, M. Lebrat, and M. Greiner, A neutral-atom Hubbard quantum simulator in the cryogenic regime, *Nature* **642**, 909 (2025).

[50] M. Fishman, S. R. White, and E. M. Stoudenmire, The ITensor Software Library for Tensor Network Calculations, *SciPost Phys. Codebases* , 4 (2022).

[51] M. Fishman, S. R. White, and E. M. Stoudenmire, Codebase release 0.3 for ITensor, *SciPost Phys. Codebases* , 4 (2022).

[52] P. A. M. Dirac, Note on exchange phenomena in the thomas atom, *Mathematical Proceedings of the Cambridge Philosophical Society* **26**, 376–385 (1930).

[53] J. Haegeman, J. I. Cirac, T. J. Osborne, I. Pižorn, H. Verschelde, and F. Verstraete, Time-dependent variational principle for quantum lattices, *Phys. Rev. Lett.* **107**, 070601 (2011).

Supplemental Material to “Controlled pairing symmetries in a Fermi-Hubbard ladder with band flattening”

João P. Mendonça,^{1, 2, *} S. Biswas,³ M. Dziurawiec,⁴ U. Bhattacharya,⁵ K. Jachymski,² M. Aidelsburger,^{6, 7, 8} M. Lewenstein,⁹ M. M. Maśka,⁴ and T. Grass^{3, 10, †}

¹Centre for Quantum Optical Technologies, Centre of New Technologies, University of Warsaw, Banacha 2c, 02-097 Warsaw, Poland

²Faculty of Physics, University of Warsaw, Pasteura 5, 02-093 Warsaw, Poland

³DIPC - Donostia International Physics Center, Paseo Manuel de Lardizábal 4, 20018 San Sebastián, Spain

⁴Institute of Theoretical Physics, Wrocław University of Science and Technology, 50-370 Wrocław, Poland

⁵Institute for Theoretical Physics, ETH Zürich, Zürich 8093, Switzerland

⁶Max-Planck-Institut für Quantenoptik, 85748 Garching, Germany

⁷Munich Center for Quantum Science and Technology (MCQST), 80799 München, Germany

⁸Fakultät für Physik, Ludwig-Maximilians-Universität, 80799 München, Germany

⁹ICFO-Institut de Ciències Fotoniques, The Barcelona Institute of Science and Technology, 08860 Castelldefels (Barcelona), Spain

¹⁰IKERBASQUE, Basque Foundation for Science, Plaza Euskadi 5, 48009 Bilbao, Spain

(Dated: December 25, 2025)

We provide additional information related to dynamical properties (spectral function, dynamical spin structure factor), to the generalized Penrose-Onsager criterion, obtained from the eigenvalue spectrum of the non-local d -wave density matrices, and on the finite-size scaling of the eigenvalue gaps.

S1. SPECTRAL FUNCTION

The single-particle spectral function $A(\mathbf{q}, \omega)$ can be obtained by computing the nonequal time two-point correlators via a real-time evolution. To this end, we time evolve the ground state through a local quench, from which the dynamical correlation functions can be extracted at each time step. Thus,

$$A_\sigma(\mathbf{q}, \omega) = \sum_j e^{-i\mathbf{q} \cdot \mathbf{r}_j} \times \frac{1}{2\pi} \left[\int_{-\infty}^{\infty} dt e^{i(\omega - E_0)t} \langle c_{j\sigma}(t) c_{0\sigma}^\dagger(0) \rangle + \int_{-\infty}^{\infty} dt e^{-i(\omega + E_0)t} \langle c_{j\sigma}^\dagger(t) c_{0\sigma}(0) \rangle \right], \quad (\text{S1})$$

where the expectations are taken in the ground state whose energy is E_0 . Here, we performed the time evolution using the time-dependent variational principle method [1, 2].

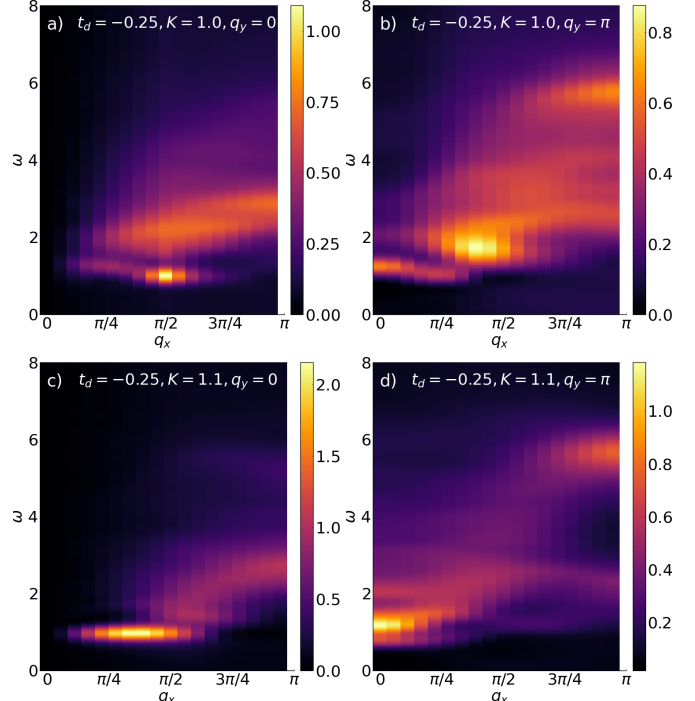


FIG. S1. Dynamical spin structure factor $S^{zz}(\mathbf{q}, \omega)$ for $t_d = -0.25$, $K = 1.0$ [(a) and (b)] and $K = 1.1$ [(c) and (d)]. Results are presented for $q_y = 0$ [(a) and (c)] and $q_y = \pi$ [(b) and (d)].

S2. DYNAMICAL SPIN STRUCTURE FACTOR.

The dynamical spin structure factor $S^{zz}(\mathbf{q}, \omega)$ is written as

$$S^{zz}(\mathbf{q}, \omega) = \sum_j e^{-i\mathbf{q} \cdot \mathbf{r}_j} \int_{-\infty}^{\infty} dt e^{i\omega t} \langle S_j^z(t) S_0^z(0) \rangle. \quad (\text{S2})$$

* jpedromend@gmail.com

† tobias.grass@dipc.org

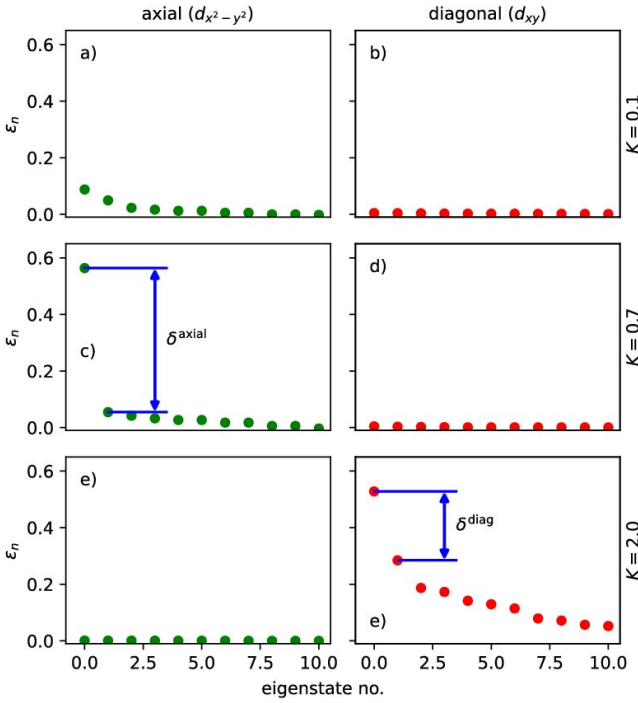


FIG. S2. The lowest 10 eigenvalues of the density matrices $G^{x^2-y^2}$ [(a), (c), (e)] and G^{xy} [(b), (d), (f)] [cf. Eqs. (3a) and (3b) for $t_d = -0.25$ and $K = 0.1$ [(a), (b)], $K = 0.7$ [(c), (d)], and $K = 2.0$ [(e), (f)]. The system size is 30×2 .

Figure S1 shows an example of how $S^{zz}(\mathbf{q}, \omega)$ changes when we go from $K = 1.0$ to $K = 1.1$, that is, when the system goes from the $d_{x^2-y^2}$ -wave phase to the d_{xy} -wave phase. Clearly, for $q_y = \pi$, the maximum weight of $S^{zz}(\mathbf{q}, \omega)$ abruptly shifts from a finite q_x to $q_x = 0$. Similar changes can also be observed for other transitions, which were used as additional indicators of phase transitions.

S3. GENERALIZED PENROSE-ONSAGER CRITERION.

We show in Fig. S2 the highest eigenvalues of the d -wave correlations, given by Eqs. (3a) and (3b). In all panels, we set $t_d = -0.25$ and choose $K = 0.1$ in panel (a,b), 0.7 in panel (c,d), and 2.0 in panel (e,f). These parameters correspond to the three different phases observed in our model. For small K , panels (a) and (b), no eigenvalue dominates the spectrum, and hence, neither diagonal nor axial pairs are condensed. In contrast, at an intermediate K , panels (c) and (d), a pronounced eigenvalue emerges in the eigenvalue spectrum of the axial $d_{x^2-y^2}$ -wave pairing. Finally, for a strong K , panels (e) and (f), a dominant eigenvalue appears in the diagonal d_{xy} -wave pairing correlations. Consequently, the

eigenvalue gap between the largest and second-largest, denoted δ^{axial} and δ^{diag} , respectively, can be used as order parameters of the different pairing phases, as also done in Fig. 5 of the main text.

S4. EFFECT OF FINITE SYSTEM SIZE.

The finite-size analysis of the gaps shown in Fig. S3. A comparison of the magnitude of the eigenvalue gap for systems of different sizes indicates that the systems used in the calculations presented in this work (36×2 for the spectral functions and dynamical spin structure factors and 30×2 for the other quantities) are large enough to determine the phase boundaries within the error bars marked in Fig. 5.

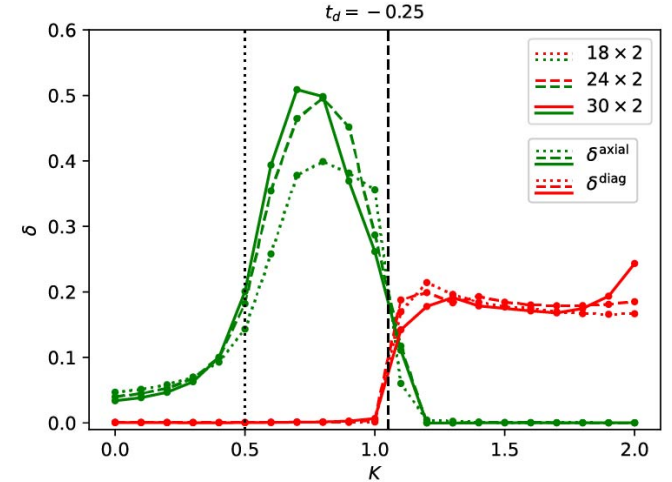


FIG. S3. The magnitude of the eigenvalue gap for 18×2 (dotted lines), 24×2 (dashed lines), and 30×2 (solid lines) systems for $t_d = -0.25$. The green lines show δ^{axial} and the red lines show δ^{diag} .

S5. PAIRING GAP

In order to estimate the magnitude of the pairing gap, we calculate the binding energy of a pair of electrons,

$$\Delta E_B = 2E_0(N_e + 1) - E_0(N_e + 2) - E_0(N_e), \quad (S3)$$

where $E_0(N)$ is the energy of the groundstate in a system with N particles and N_e is the number of particles corresponding to the filling $\rho = 1/3$ considered in this work. It can be intuitively understood as the energy cost difference of adding two independent electrons instead of a pair. In Fig. S4 we show that ΔE_B indicates gap opening in the axial $d_{x^2-y^2}$ -wave pairing phase.

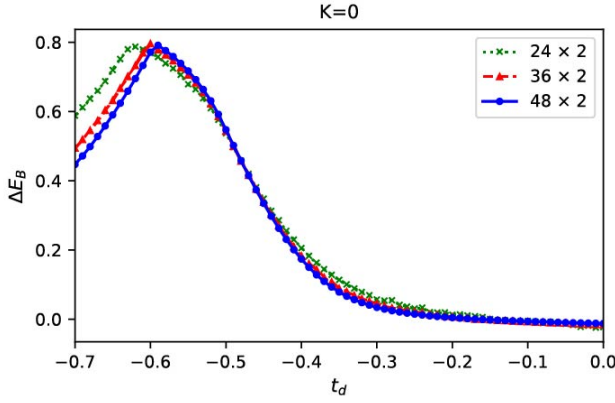


FIG. S4. The magnitude of the binding energy (S3) for three system sizes $L_x = 24$ (green), $L_x = 36$ (red), $L_x = 48$ (blue) at $K = 0$.

[1] P. A. M. Dirac, Note on exchange phenomena in the thomas atom, *Mathematical Proceedings of the Cambridge Philosophical Society* **26**, 376–385 (1930).

[2] J. Haegeman, J. I. Cirac, T. J. Osborne, I. Pižorn, H. Verschelde, and F. Verstraete, Time-dependent variational principle for quantum lattices, *Phys. Rev. Lett.* **107**, 070601 (2011).